Epitaxial molybdenum oxide grown on Mo(110): LEED, STM, and density functional theory calculations

K. Radican,* N. Berdunov,† G. Manai, and I. V. Shvets
CRANN, School of Physics, Trinity College, Dublin 2, Ireland
(Received 10 July 2006; revised manuscript received 6 December 2006; published 27 April 2007)

The oxidation of Mo(110) was studied at 1000 °C and 1×10^{-6} Torr oxygen. Low energy electron diffraction and scanning tunneling microscopy data were used to give a detailed analysis of the oxide surface structure. From this data a model was built, and through the use of density functional theory (DFT) calculations, we show that a strained bulklike $MoO_2(010)$ "surface oxide" is in excellent agreement with the experimental data. The stability of this oxide was accounted for by a strong adhesion at the interface. The origin of this strong adhesion between the film and substrate can be related to the charge redistribution at the interface, which is analogous to the macroscopic image charge interaction between the two. Furthermore, we employed DFT calculations to illustrate the charge redistribution at the interface and estimate the work of adhesion for this system. The calculated work of adhesion is around 7 J/m^2, indicating that there is indeed a strong interaction between the film and substrate as expected.

DOI: 10.1103/PhysRevB.75.155434 PACS number(s): 68.35.Bs, 81.65.Mq, 68.37.Ef, 68.43.Bc

I. INTRODUCTION

The oxide formation on transition metal (TM) surfaces has been receiving considerable attention in recent years.[1–4] Understanding the mechanisms of the initial growth stages of these oxides is necessary for both, fundamental understanding of science and advanced technologies. These oxides are important in many areas of industry, including surface coatings, materials science, and for industrial catalysts used in oxidation reactions for fuel processing, chemical production, and pollution cleanup. Recently, considerable steps have been made in the microscopic understanding of oxide formation on TM surfaces. With new advancements in computer technology, researchers have been able to gain vast insight in the formation of these oxides by combining experimental data with density functional theory (DFT) calculations.[1–10] These calculations have led to some rather complex models for the initial oxide formation that may or may not represent the bulk oxide. For late transition metals and noble metals such as Pd and Ag it is now known that the oxidation process proceeds through ultrathin oxide layers, that are thermodynamically stable.[11–14] It is unclear whether the same holds true for TM's further to the left in the periodic table. The recent theoretical and experimental studies on the initial oxidation stages of Pd(111), Pd(100), Rh(111), Rh(110), and Rh(100) show that the structures of the surface oxides differ from those of the bulk oxides.[1,2,12,14,15] The surface oxides on these metals exhibit different thermodynamic stabilities. A common feature is that their formation involves subsurface penetration of oxygen, thus the metal atoms of the surface oxide are sandwiched between two atomic layers of oxygen, forming oxygen-metal-oxygen (O-M-O) trilayer surface oxides. Thus far the recent studies of the surface oxidation of the 4*d* series span from Ag to Rh. Within this span there is a developing trend from a thermodynamically stable (O-M-O) surface oxide trilayer for Ag, to a slightly less stable trilayer for Pd, to a transient, kinetically stable trilayer for Rh. However, it was recently suggested that since many of the TM oxides wet their own metal surfaces, the adhesion energy should provide extra stabilization allowing a bulklike surface oxide to form when the O_2 partial pressure is many orders of magnitude lower than required to maintain the bulk oxide.[3]

In response to this we targeted the lighter metals of the 4*d* series to establish if a bulklike surface oxide exists on the molybdenum surface, and if so then what is the epitaxial relationship between the film and substrate.

II. EXPERIMENT

We used single crystal Mo(110) with the surface deviation from the (110) plane of less than 0.1°. The substrate was placed in an ultrahigh vacuum (UHV) chamber of base pressure below 10^{-10} Torr. The chamber is equipped with low energy electron diffraction (LEED), Auger electron spectroscopy (AES), and scanning tunneling microscopy (STM). The Mo substrates were first cleaned using the procedure established by Haas and Jackson.[16] This procedure is based on annealing the substrate in an O_2 atmosphere of 1×10^{-6} Torr followed by a series of high-temperature flashes to remove the surface oxides. The Mo substrate was annealed at 1000 °C for 1 hour at 10^{-6} Torr. The chamber was then pumped down to UHV and the sample was flashed several times to 1600 °C for 30 seconds. This process was repeated until a clean Mo surface was obtained as checked with AES, and a Mo(110) $p(1\times1)$ LEED pattern was imaged. For these experiments the ultrapure oxygen was introduced to the chamber via a leak valve. The sample was heated via electron beam bombardment and temperatures were measured with an optical pyrometer.

Once a clean surface was obtained the samples were annealed to 1000 °C in an oxygen environment of 1×10^{-6} Torr for up to 1 minute. The surfaces were then characterized using LEED and STM. All STM images were recorded at room temperature in the constant current mode using currents of approximately 0.05 to 0.1 nA and bias voltages of 0.1 to 0.05 V with electrochemically etched W tips.

III. RESULTS AND DISCUSSION

A. Low energy electron diffraction

Figure 1 shows the LEED pattern of the molybdenum oxide overlayer on the Mo(110) surface after annealing at

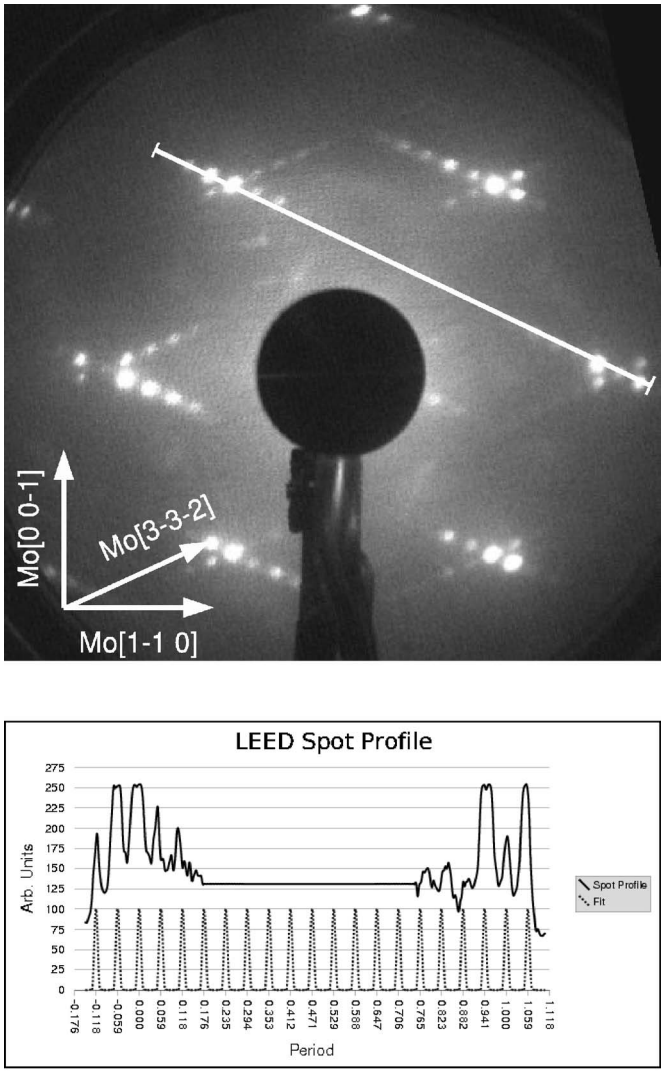

FIG. 1. The LEED pattern of the oxide overlayer on Mo(110) taken at 103 eV. The sample was annealed for 30 s at 1000 °C and 1×10^{-6} Torr oxygen pressure. Below is a graph of a spot profile taken along the row of satellite spots indicated by the white line on the LEED image. The graph shows two curves. The curve above shows the LEED spot profile with the amplitude corresponding to the intensity of the LEED pattern. The curve below is a fit of the above profile showing the satellites have 1/17th the periodicity as the $p(1\times1)$ spots.

1000° C and 1×10^{-6} Torr for 30 seconds, and then cooled in an O_2 environment at a rate of ~200 °C/min. The LEED pattern shows two rows of satellite spots that form an X shape centered about the molybdenum $p(1\times1)$ spots. The rows are separated by an angle of 50° that is bisected by the Mo[1-1 0] direction. Using the Mo(110) $p(1\times1)$ LEED pattern of the substrate as our reference, we determined that the rows are running along the Mo[3-3 2] and Mo[3-3-2] direction. The pairing of these rows along two equivalent directions is an indication of the overlapping of patterns of two equivalent overlayer domains.

A spot profile along one of these rows is shown by the graph below the LEED image in Fig. 1. This profile shows that the satellite spots have a periodicity of 1/17 of the spacing between two primary Mo(110) LEED spots. From the direction and period of the rows it was determined that the satellite spots correspond to an overlayer with dimensions in the real space of 5.2 Å along the [1-1-3] direction (orthogonal to [3-3-2]). This 5.2 Å separation is equal to one spacing of Mo lattice in that direction. Furthermore, we can say that this 1:1 coincidence reoccurs once for every 17 units in the Mo[0 0-1] direction. This corresponds to a separation of ~23 Å between two rows of coincidence. The same applies to the equivalent [1-1 3] direction of the Mo lattice. We can therefore conclude that there is 1:1 coincidence between the overlayer and the Mo substrate in these two directions. For that reason we will assign the domains to be lying along the [1-1-3] and [1-1 3] directions, and for simplicity the description will be kept to the Mo[1-1-3] domain. The matrix describing the coincidence unit cell is then

$$\begin{bmatrix} 17 & -17 \\ 2 & 1 \end{bmatrix}.$$

As an aid the real and reciprocal space diagrams of this system are illustrated in Fig. 2. In this figure the real and reciprocal space Mo(110) unit vectors are labeled a_1 and a_2, and a_1^* and a_2^*, respectively. The real and reciprocal space unit vectors of the overlayer are labeled b_1 and b_2, and b_1^* and b_2^*, respectively.

B. Scanning tunneling microscopy

Figure 3 presents an STM image of the surface of Mo(110) after annealing under the same conditions discussed above. This image shows a periodic row structure aligned along the Mo[1-1-3] direction. This row structure has a period of 23±1 Å and corrugation of 0.2±0.1 Å. These rows are highly regular and seemingly cover the entire substrate surface. The periodicity and direction of these rows is consistent with the spacing of the satellite spots in the LEED pattern shown in Fig. 1. The image (b) in Fig. 3 was taken at a bias of 0.05 V and is a zoom of the area in the top right of Fig. 3(a). It shows that the atomic surface structure has a quasihexagonal surface mesh with a lattice constant of 5.7±0.2 Å and an angle of ~124°. This mesh is highlighted by the white diamond, and the atomic structure which is highlighted by the white dots on this diamond. These dots have a periodicity of 2.9±0.1 Å along the side marked *a*, forming rows in a direction that is near to Mo[0 0-1]. There is a modulation in the intensity, or height, of the atoms along the rows as shown in the line profile below the image in Fig. 3. Furthermore, these rows are separated by 5.7±0.2 Å in a direction near to Mo[1-1 1], marked side *b* of the diamond. It should be noted that this surface structure is the same over the the entire surface; however, most areas needed to be enhanced with FFT filtering before it becomes obvious.

Given that the periodicity and direction of these rows is the same as the coincident lattice structure seen with LEED, we consider that the rows represent the coincidence molybdenum oxide structure. It has been shown in previous studies of coincident lattice structures using electron-scattering quantum chemistry (ESQC) that the atomic contrast of an

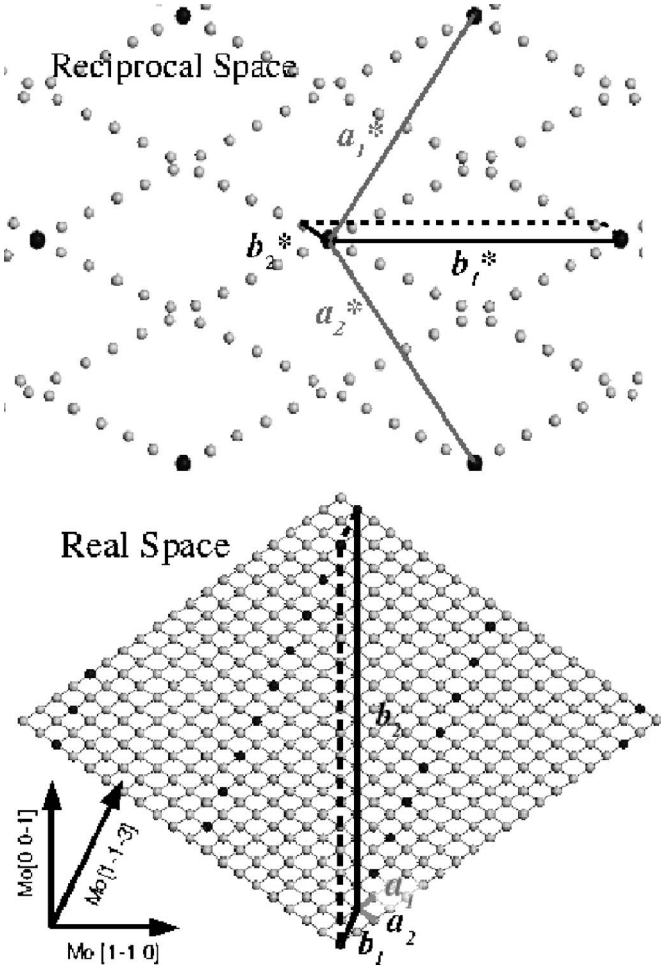

FIG. 2. Unit vectors along Mo[1-1-1] and Mo[1-1 1] in the real and reciprocal space are labeled a_1 and a_2, and a_1^* and a_2^*, respectively. The overlayer real and reciprocal space unit vectors are labeled b_1 and b_2, and b_1^* and b_2^*, respectively. The black dotted line along the b_1 direction represents the 1:1 coincidence of the overlayer and substrate in the Mo[1-1-3] direction.

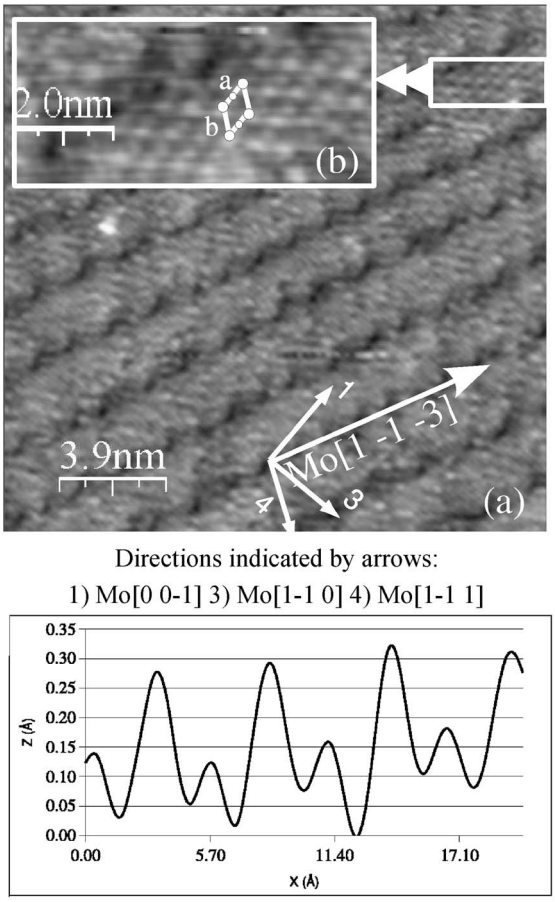

FIG. 3. (a) STM image taken at a bias of 0.10 V and current of 0.1 nA of the MoO_2/Mo(110) surface after annealing for 30 s at 1000 °C and 1×10^{-6} Torr oxygen pressure. The image shows a periodic row structure aligned along the Mo[1-1-3] direction with a period of 23±1 Å. (b) Is a zoom of the area indicated by the box in the top right of the figure, taken at bias of 0.05 V and current of 0.1 nA. A white diamond with white dots highlights the atomic surface structure. These dots have a periodicity of 2.9±0.1 Å along the side marked *a*, forming atomic rows in the ~Mo[0 0-1] direction. There is a modulation in the intensity, or height, of the atoms along the rows. This modulation is shown by a line profile taken along a row, and is illustrated in the graph below the image. Furthermore, these rows are separated by 5.7±0.2 Å in a direction near to Mo[1-1 1] marked side *b* of the diamond.

STM image of an ultrathin oxide layer on a metal substrate is dependent on the site location of the oxygen atom on the substrate.[17] This was explained by an interplay of several electronic effects causing a difference in the tunneling probability at that location. This theory has been used to explain the Moire patterns that are often seen by STM with coincidence lattice structures,[11,17–21] and can explain the striped pattern shown in Fig. 2. With this in mind and from what we know from the LEED and STM data a model for this system was developed.

C. MoO_2 surface oxide model

Based on previous Raman, XPS and RHEED studies of the oxidation of molybdenum it was determined that MoO_2 is the sole oxide that grows epitaxially on the Mo(110) surface at low pressures.[16,22–28] The MoO_2 bulk structure has a monoclinic-distorted rutile structure (space group $P21/C$) with lattice parameters a=5.661 Å, b=4.846 Å, c=5.628 Å, and β=120.95°.[29] This gives the a and c axes and the angle β dimensions similar to the overlayer imaged by STM. Also, the axes are nearly 2 times that of the Mo bulk lattice constant with β close to the angle of the quasihexagonal Mo(110) surface. Because of this, there are multiple epitaxial relationships that are suitable matches for the LEED data. However, considering the size and shape of the surface mesh imaged by STM the only compelling overlayer structure is MoO_2(010)/Mo(110). The MoO_2(010) surface is a quasihexagonal surface with a lattice spacing on the order of 5.7 Å and an angle of 120.95°, and very similar to the surface imaged STM. Furthermore, the MoO_2(010) surface (Fig. 3) is built from alternating ionic planes of oxygen anions, and Mo-Mo bonded dimers (Fig. 4). A layered oxygen-metal-oxygen (O-M-O) surface like this is a likely choice for

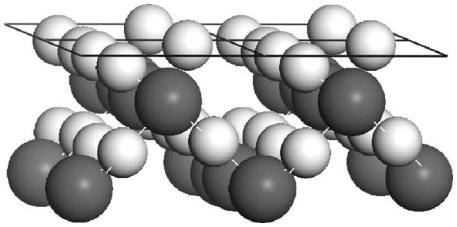

FIG. 4. The $MoO_2(010)$ surface is built from alternating layers of oxygen anions (white) and Mo-Mo bonded cations (gray). In the oxygen layers the oxygen is arranged in quasihexagonal pattern with an atomic spacing of ~3 Å. In the Mo layers the metal forms dimers that are aligned along the $MoO_2[100]$ direction, and are arranged in quasihexagonal pattern with dimensions of the MoO_2 unit cell.

two reasons. First, metal-polar-oxide interfaces such as this, where the oxide has only oxygen ions within the terminating plane are generally considered most stable, with adhesive energies an order of magnitude higher than nonpolar interfaces.[1–10,14,18,30,31] This stability is believed to arise from several factors including the macroscopic Coulomb interaction between the ions in the oxide and the image charges in the metal.[30,31] On the atomic scale this interaction is better described by a charge redistribution across the interface.[32,33] In addition to this, several studies of the surface oxides of TM's have shown through a combination of LEED and DFT that a O-M-O trilayer can be the most energetically favored.[1,2,12,14,15]

Using the literature as our inspiration we started with a MoO_2 O-M-O trilayer, and considered the interface as being built from the Mo(110) surface plane followed by the $MoO_2(010)$ oxygen plane. We started by orientating the $MoO_2(010)$ oxygen plane to find a suitable match with the Mo(110) surface mesh that formed 1:1 coincidence about the Mo[1-1-3] direction. Since the Mo(110) surface mesh and the $MoO_2(010)$ oxygen mesh are both quasihexagonal with similar lattice parameters there are three suitable orientations that form such coincidence, MoO_2 either [201] or [-101] or [102] are parallel to Mo[1-1-3]. The next step was to compare these three models to the LEED and STM in order to narrow the selection. Upon fitting the three possible orientations into a unit cell constrained by the dimensions determined by LEED the possible orientations were narrowed to one, the $MoO_2[201] \| Mo[1\text{-}1\text{-}3]$ orientation. This selection was done by considering two things. First we chose only those orientations with a minimal amount of stress induced on the film to fit the unit cell, and more importantly this was the only orientation with an equivalent domain along Mo[1-1 3] direction. With this orientation the MoO_2 *c* axis is orientated 4.9° off the Mo[0 0-1] direction, and the *a* axis near to the Mo[1-1 1]. There is an equivalent domain of MoO_2(0-1 0) [2 0 1] ‖ Mo[1-1 3] with the *c* axis orientated the same degree off the Mo[0 0-1] but in the opposite direction, and the *a* axis near the equivalent Mo[1-1-1] direction.

The next step was to optimize this model to completely agree with the LEED and STM data. In order to induce the required 1:1 coincidence Mo [1-1-3] that reoccurs once every 17 units along Mo[0 0-1] the overlayer was skewed by

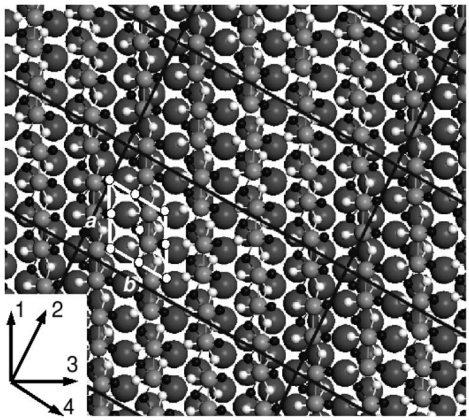

Directions indicated by arrows:
1) Mo[0 0-1] 2) Mo[1-1-3] 3) Mo[1-1 0] 4) Mo[1-1 1]

FIG. 5. Top view of the $MoO_2(010)$ overlayer unit cell as determined by STM, LEED, and DFT calculations. The larger dark gray spheres represents the Mo(110) surface atoms, the white spheres represent the O^{2-} interface atoms, the gray spheres represent the Mo^{4+} atoms, and the black spheres represent the O^{2-} surface atoms. The black rectangular grid represents the overlayer unit cell. Note that this is the "on-top" configuration and that the interface oxygen atoms are located on top of the Mo interface atoms at the intersections of the grid lines and along the Mo [1-1-3] direction.

2.7°. After the skewing the MoO_2 [100] is now 2° off the Mo[0 0-1], and the overlayer can be described by a unit cell of MoO_2[201] parallel to Mo[1-1-3] and MoO_2[0 0 4] parallel to one-half a unit of Mo[9-9 7]. The dimensions of such a unit cell are 10.4 Å × 22.9 Å with an angle of 86.4°. Furthermore, the matrix describing the overlayer unit cell can be reduced to cell dimensions of the smallest length scale describing the overlayer as

$$\begin{bmatrix} 1 & 8 \\ -4 & 2 \end{bmatrix}.$$

The illustration in Fig. 5 shows the $MoO_2(010)/Mo(110)$ surface model as described above. The black mesh shows the overlayer unit cell in agreement with the LEED data. There is a 1:1 coincidence between the interfacial oxygen and molybdenum atoms that runs along the Mo[1-1-3] direction (along the black mesh lines in that direction). The white diamond highlights the surface oxygen unit cell, and the surface oxygen are highlighted in that cell by the white dots. The surface oxygen unit cell is in perfect agreement with the STM data except there is an added row of oxygen running along the *a* axis [side marked (a) in Fig. 3].

D. Density functional theory calculations

To further refine this model DFT calculations were carried out. As a first approximation the MoO_2 unit cell was given a slight distortion and rotation to align the *a* and *c* axes along Mo [1-1-1] and [0 0-1], respectively (Fig. 6). To fit the oxide to the substrate the oxide unit cell was skewed by 4° to give an angle of 125°, the *a* axis was reduced by 3%, and the

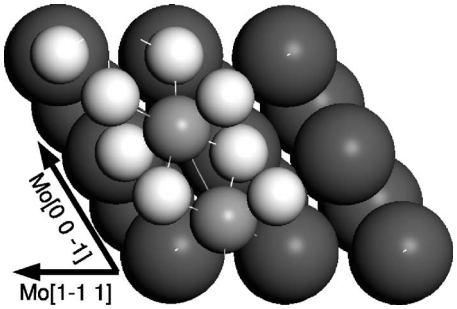

FIG. 6. Model unit cell used for DFT calculations with $MoO_2(010)$ plane parallel to the Mo(110) surface and $MoO_2(010)$ the *a* and *c* axes aligned along the Mo[1-1-1] and [0 0-1], respectively.

c was stretched by 10%. In doing this we were able to fit one primitive unit cell of the $MoO_2(010)$ surface to the Mo(110) surface, greatly reducing our computing cost. This modification also allows us to compare the four possible interfacial oxygen coordination sites at the interface in terms of energy, work of adhesion, and interlayer separation. For the calculations we used a periodic slab geometry with a four layer slab of Mo(110), an O-Mo-O trilayer of $MoO_2(010)$, and a vacuum gap of 15 Å between the slabs to eliminate any spurious electric fields.[7] In these calculations the bottom two layers of the Mo slab were constrained and the top two Mo layers along with MoO_2 were allowed to relax. These calculations were performed using CASTEP,[34] and for comparison both the generalized gradient approximation (GGA) and the local density approximation (LDA) with a cutoff of 300 eV and a *k*-point separation of 0.05–1/Å in the Brillouin zone were used. We calculated the work of adhesion as the difference of the sum of the individual energies of the relaxed Mo(110) and $MoO_2(010)$ slabs and the energy of the two interfaced together, all divided by the area of the interface. DFT geometry optimizations were performed for the slabs of dimensions shown in Fig. 6 for each of the four possible configurations of the interfacial oxygen. These configurations are (a) on the two-fold bridge site above the underlying Mo atom, (b) atop the surface Mo, (c) on the three-fold hollow site, and (d) two-fold bridge site no underlying Mo atom (Fig. 7).

It was found that both of the bridge configurations, (a) and (d), relaxed on to the three-fold site, leaving us with only two stable configurations. In both cases there was a strong adhesion between the film and substrate, as expected for a polar oxide-metal interface. The adhesion energy from this system has two main components, a contribution from the metal-oxygen bonding, and a contribution arising from the electron redistribution at the interface. The latter is the result of the metal substrate transferring electrons to the interfacial oxygen atoms, which can be explained by the Pauling's electronegitivity of the two elements, $\chi_{Mo}(1.8) < \chi_O(3.5)$. This results in a polarization of the metal at the interface, and a stronger adhesion energy. This effect was found to increase the adhesion energy an order of magnitude for the polar Mo/MgO(111) interface compared to the nonpolar Mo/MgO(100) interface.[35] A map of the electron density difference gives an illustration of the electron redistribution

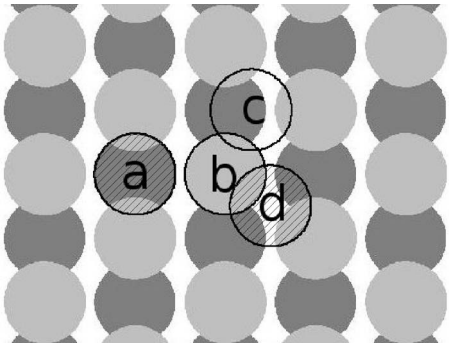

FIG. 7. DFT geometry optimizations were performed for each of the four possible configurations of the interfacial oxygen atoms that form the coincident sites seen in the LEED data. These configurations are (a) on the two-fold bridge site above the underlying Mo atom, (b) atop the surface Mo, (c) on the three-fold hollow site, and (d) two-fold bridge site no underlying Mo atom.

at the interface for the two configurations (Fig. 8). On this map the light areas above the interface oxygen indicate an enhanced electron population, whereas the dark areas and bands above the Mo atoms and along the interface indicate a reduced electron population, thus mimicking the macroscopic image charge. Furthermore, with these two configurations it was found that the case with the interface oxygen located on the three-fold site had the lowest energy by 0.20 and 0.23 eV per atom at the interface as calculated by GGA

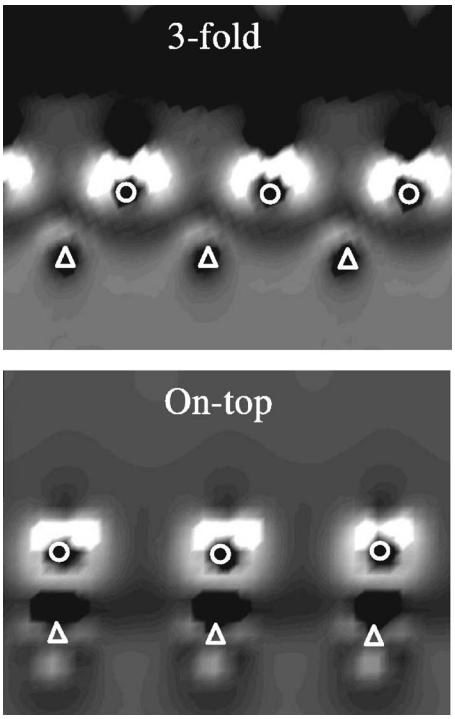

FIG. 8. A slice taken along the Mo(1-1 0) surface showing a map of the electron density difference for the three-fold and on-top configuration. The circles mark the interfacial oxygen and the triangles mark the substrate Mo locations. Light areas represent positive and dark areas represent negative areas corresponding to enhanced and reduced electronic populations, respectively. This map was generated using the results of the GGA calculations.

TABLE I. DFT geometry calculations.

Configuration	ΔE (eV/atom)[a] GGA	ΔE (eV/atom)[a] LDA	W (J/m^2)[b] GGA	W (J/m^2)[b] LDA	Interlayer separation (Å) GGA
Top site	0.2	0.23	5.75	6.48	1.72
Three-fold			7.13	8.10	1.18

[a]ΔE is the difference in total energy for the system.
[b]W is the work of adhesion.

and LDA, respectively. This configuration also had the shortest interlayer separation and highest work of adhesion, indicating a stronger interface bonding; the results of these calculations are shown in Table I.

From these results full overlayer unit cell slabs for both the on top and three-fold configurations were constructed. These slabs consisted of two layers of Mo(110) and the MoO_2(010) trilayer giving 148 atoms in total. The interlayer distance at the interface was fixed across the slab to the value calculated for the respective configurations (i.e., interlayer warping was not considered for the different configurations across the interface[10]). The unit cell slab used for the on-top configuration is shown in Fig. 5.

DFT calculations using the LDA and an energy cutoff of 300 eV were performed for the two cases. It was found that the three-fold case converged with an energy of 0.1 eV/atom lower than the on-top case, suggesting that this is the most stable surface. STM simulations of the two DFT calculations using a tip to sample bias of 0.05 V were also performed. The case of the three-fold site configuration showed obvious row structures formed by the STM contrast, in agreement with the rows seen in the STM data. However, the on-top site configuration showed very little change in contrast. An STM simulation for the three-fold case is compared with an atomically resolved STM image of the MoO_2(010)/Mo(110) surface. The comparison shows that this model is now in excellent agreement with the STM data (Fig. 9). Again to highlight the surface oxygen unit cell a white diamond is drawn, with the surface oxygen in the cell represented by white dots. The oxygen lattice in this simulation features a missing row of oxygen along the MoO_2[1 0 0], as in the STM data. Furthermore, there is also an alternation of the bright and dim spots that represent the oxygen atoms along the rows in agreement with the experimental data.

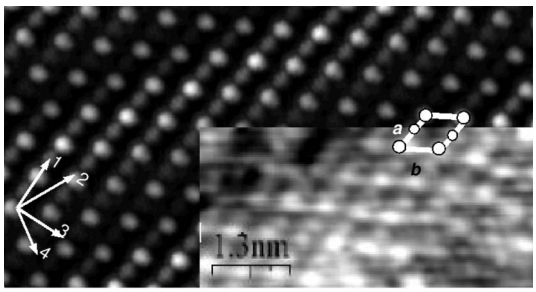

Directions indicated by arrows:
1) Mo[0 0-1] 2) Mo[1-1-3] 3) Mo[1-1 0] 4) Mo[1-1 1]

FIG. 9. The high resolution STM image taken at 0.05 V and 0.1 nA in constant current mode (lower left) compared with a DFT STM simulation at 0.05 V. The MoO_2(010) atomic surface structure has a quasihexagonal surface mesh with a lattice constant of 5.7±0.2 Å and an angle of ~124°. This mesh is highlighted by the white diamond, and the atomic structure is highlighted by the white dots on this diamond. These dots have a periodicity of 2.9±0.1 Å along the side marked *a* (*a* axis), forming rows in a direction that is near to Mo [0 0-1]. There is a modulation in the intensity, or height, of the atoms along the rows. Furthermore, these rows are separated by 5.7±0.2 Å in a direction near to Mo[1-1 1], marked side *b* of the diamond (*c* axis). The brightest spots are located above areas where the oxygen atoms at the interface are located on the three-fold hollow sites.

Further investigation of the STM simulation of the three-fold case reveals the origin of both the bright and dim STM spots of the surface oxygen atoms along the MoO_2 *a* axis, along with the origin of the missing oxygen row seen in the STM data. Figure 10 shows the map of STM simulation from Fig. 9 overlaid on the model of the MoO_2 (010) surface. This figure shows that the dim spots on the STM images are a probe of the empty states near the Fermi level in the molecular orbital of the O^{2+} surface atoms that bridge between two Mo atoms of separate Mo dimers, marked (a), whereas the bright spots (b) are representative of the states in the molecular orbital of the O^{2+} surface atoms that bridge the two Mo atoms forming Mo-Mo dimers. This indicates that the density of states accessible by the STM tip is more localized around these areas marked (b), and can be related to bulk MoO_2 where the atomic sphere radii for the oxygen located in this position was calculated to be ~10% larger versus the oxygen bonded to the Mo dimers.[36] Furthermore, the oxygen atoms of type marked (c) in the figure have a single bond to the Mo and are not imaged by STM.

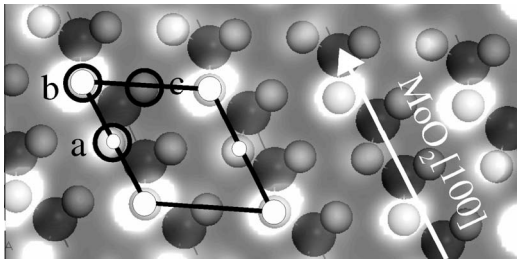

FIG. 10. Overlay of an STM simulation at 0.05 V for the three-fold case. The MoO_2 unit cell is drawn by the black diamond, and the surface oxygen are white, and first layer of molybdenum atoms are gray. The circle marked (a) shows the dim oxygen atoms seen in STM, circle (b) shows the bright oxygen atoms, and circle (c) shows the missing oxygen atoms.

IV. SUMMARY AND CONCLUSIONS

The oxidation of Mo(110) was studied and it was found that a bulklike oxide of $MoO_2(010)$ grows epitaxially on the surface at 1000 °C and 1×10^{-6} Torr oxygen pressure. LEED and STM data were used to give a detailed analysis of the oxide surface structure. From this experimental data a model was built and through the use of DFT calculations we show that a strained bulklike $MoO_2(010)$ film is in excellent agreement with the experimental data. The coincidence structure can be described in matrix notation by

$$\begin{bmatrix} 1 & 8 \\ -4 & 2 \end{bmatrix}$$

giving a MoO_2 overlayer with $MoO_2[201]\|Mo[1\text{-}1\text{-}3]$ and $MoO_2[100]\|Mo[00\text{-}1]$. The oxide overlayer is strained by ~5.5% and skewed by 4.9°. The DFT calculations suggest that the most stable configuration for the interfacial oxygen is in the three-fold coordination. Furthermore, it was found that while this oxide phase readily grew into thicker three-dimensional MoO_2 single crystalline thin films, only the surface oxide was stable up to 1000 °C in UHV. This indicates that there is an increase in thermodynamic stability given by the adhesion energy. The origin of this strong adhesion between the film and substrate can be related to the charge redistribution at the interface, and has been calculated for many metal-oxide systems with various *ab initio* methods.[8,32,33] An electron density difference map of the interface was used to illustrate the charge redistribution for this system. Furthermore, we employed DFT calculations to estimate the work of adhesion for this system and there is indeed a strong interaction between the film and substrate as expected. The calculated work of adhesion is around 7 J/m^2.

ACKNOWLEDGMENTS

This work made use of computing facilities at the Trinity Centre for High Performance Computing, supported by IITAC, the HEA, and the National Development Plan.

*Electronic address: radicak@tcd.ie
†Current address: School of Physics and Astronomy, University Park, NG7 2RD, Nottingham.

[1] J. Gustafson, A. Mikkelsen, M. Borg, E. Lundgren, L. Kohler, G. Kresse, M. Schmid, P. Varga, J. Yuhara, X. Torrelles *et al.*, Phys. Rev. Lett. **92**, 126102 (2004).
[2] J. Gustafson, A. Mikkelsen, M. Borg, J. N. Andersen, E. Lundgren, C. Klein, W. Hofer, M. Schmid, P. Varga, L. Kohler *et al.*, Phys. Rev. B **71**, 115442 (2005).
[3] C. T. Campbell, Phys. Rev. Lett. **96**, 066106 (2006).
[4] M. Todorova, W. X. Li, M. V. Ganduglia-Pirovano, C. Stampfl, K. Reuter, and M. Scheffler, Phys. Rev. Lett. **89**, 096103 (2002).
[5] A. Stierle, F. Renner, R. Streitel, H. Dosch, W. Drube, and B. C. Cowie, Science **303**, 1652 (2004).
[6] D. J. Siegel, L. G. Hector, Jr., and J. B. Adams, Phys. Rev. B **65**, 085415 (2002).
[7] R. Benedek, M. Minkoff, and L. H. Yang, Phys. Rev. B **54**, 7697 (1996).
[8] M. W. Finnis, J. Phys.: Condens. Matter **8**, 5811 (1996).
[9] J. Purton, S. C. Parker, and D. W. Bullett, J. Phys.: Condens. Matter **9**, 5709 (1997).
[10] R. Benedek, A. Alavi, D. N. Seidman, L. H. Yang, D. A. Muller, and C. Woodward, Phys. Rev. Lett. **84**, 3362 (2000).
[11] C. I. Carlisle, D. A. King, M.-L. Bocquet, J. Cerdá, and P. Sautet, Phys. Rev. Lett. **84**, 3899 (2000).
[12] E. Lundgren, G. Kresse, C. Klein, M. Borg, J. N. Andersen, M. De Santis, Y. Gauthier, C. Konvicka, M. Schmid, and P. Varga, Phys. Rev. Lett. **88**, 246103 (2002).
[13] W.-X. Li, C. Stampfl, and M. Scheffler, Phys. Rev. Lett. **90**, 256102 (2003).
[14] K. Reuter and M. Scheffler, Appl. Phys. A: Mater. Sci. Process. **A78**, 793 (2004).
[15] C. Dri, C. Africh, F. Esch, G. Comelli, O. Dubay, L. Kohler, F. Mittendorfer, G. Kresse, P. Dudin, and M. Kiskinova, J. Chem. Phys. **125**, 094701 (2006).
[16] M. Kamei, T. Obayashi, H. Tsunematsu, Y. Tanaka, and Y. Gotoh, Surf. Sci. **356**, 137 (1996).
[17] Y. J. Kim, C. Westphal, R. X. Ynzunza, H. C. Galloway, M. B. Salmeron, M. A. Van Hove, and C. S. Fadley, Phys. Rev. B **55**, R13448 (1997).
[18] H. C. Galloway, P. Sautet, and M. Salmeron, Phys. Rev. B **54**, R11145 (1996).
[19] T. Maroutian, S. Degen, C. Becker, K. Wandelt, and R. Berndt, Phys. Rev. B **68**, 155414 (2003).
[20] M. Ritter, W. Ranke, and W. Weiss, Phys. Rev. B **57**, 7240 (1998).
[21] S. Degen, A. Krupski, M. Kralj, A. Langner, C. Becker, M. Sokolowski, and K. Wandelt, Surf. Sci. **576**, L57 (2005).
[22] T. Jirsak, M. Kuhn, and J. A. Rodriguez, Surf. Sci. **457**, 254 (2000).
[23] G. H. Smudde, Jr. and P. C. Stair, Surf. Sci. **317**, 65 (1994).
[24] E. Bauer and H. Poppa, Surf. Sci. **127**, 243 (1983).
[25] T. W. Haas and A. G. Jackson, J. Chem. Phys. **44**, 2921 (1966).
[26] Y. Gotoh and E. Yanokura, Surf. Sci. **287-288**, 979 (1993).
[27] A. K. Santra, B. Min, and D. W. K. Goodman, Surf. Sci. **513**, L441 (2002).
[28] T. Schroeder, J. Zegenhagen, N. Magg, B. Immaraporn, and H. Freund, Surf. Sci. **552**, 85 (2004).
[29] B. Brandt and A. Stapski, Acta Chim. Acad. Sci. Hung. **21**, 661 (1967).
[30] M. W. Finnis, Acta Metall. Mater. **40**, S25 (1992).
[31] D. M. Duffy, J. H. Harding, and A. M. Stoneham, Acta Metall. Mater. **40**, S11 (1992).
[32] C. Noguera, F. Finocchi, and J. Goniakowski, J. Phys.: Condens. Matter **16**, S2509 (2004).
[33] K. Reuter, in *Nanocatalysis: Principles, Methods, Case Studies*, edited by U. Heiz, H. Hakkinen, and U. Landman (Springer, Berlin, 2005).
[34] M. D. Segall, P. J. D. Lindan, M. J. Probert, C. J. Pickard, P. J. Hasnip, S. J. Clark, and M. C. Payne, J. Phys.: Condens. Matter **14**, 2717 (2002).
[35] J. Goniakowski and C. Noguera, Phys. Rev. B **66**, 085417 (2002).
[36] V. Eyert, R. Horny, K.-H. Höck, and S. Horn, J. Phys.: Condens. Matter **12**, 4923 (2000).